Serial dilutions of ^{18}F-FDG in a 96-well plate were imaged optically and using the aPET. A strong correlation was seen between optical signal (total flux) and aPET signal (counts) across the dilution range of 50 -1000 μCi (Supplemental Figure 1). When the same plate was imaged optically using each of the emission filters of the IVIS Lumina II, it was seen that the bulk of the photons were emitted in the 515-575 nm and 575-650 nm range, compared to the NIR range (Supplemental Figure 2).

The Cerenkov emission spectrum was examined more closely using an acrylic spherical phantom filled with 27 μCi/mL of ^{18}F-FDG. Supplemental Figure 3a shows both white light and luminescent (open filter) images of the phantom. Phantom images using each of the 4 emission filters on the IVIS Lumina II, along with their quantification, are shown in Supplemental Figure 3b. A theoretical line representing $1/\lambda^2$ is included in the plot to confirm this dependence of Cerenkov radiation on wavelength.

The emission spectrum exhibited different characteristics when Cerenkov radiation was examined in vivo. Mouse bladders were imaged one hour following administration of 435 μCi ^{18}F-FDG and the resulting image from the open filter is shown in Supplemental Figure 4a. The remaining filter sets can be seen in Supplemental Figure 4b with the quantification shown in Supplemental Figure 4c. At wavelengths greater than 575 nm, the Cerenkov emission follows the expected decrease at higher wavelengths. However, a decrease in Cerenkov intensity is seen using the lowest wavelength (515-575 nm) filter, due to attenuation and scattering by tissue.

Supplemental Figure 5 shows the change in Cerenkov emission as a function of pH measured using emission filters that fall outside the expected functional wavelength ranges of the pH indicators used. Shown are a) 25 mM PP mixed with 200 μCi ^{18}F-FDG and adjusted to pH 4-11, b) 100 μCi ^{18}F-DFPR adjusted to pH 4-7 and (c) 140 μCi ^{18}F-MFCP adjusted to pH 4-9.

Relatively little Cerenkov radiation is absorbed outside the functional wavelengths and as a result the pH dependent changes are relatively small. The expected alterations due to the dependence of Cerenkov emission on wavelength are preserved, with filters in the blue-green range showing higher Cerenkov emission that those in the red and near-infrared.

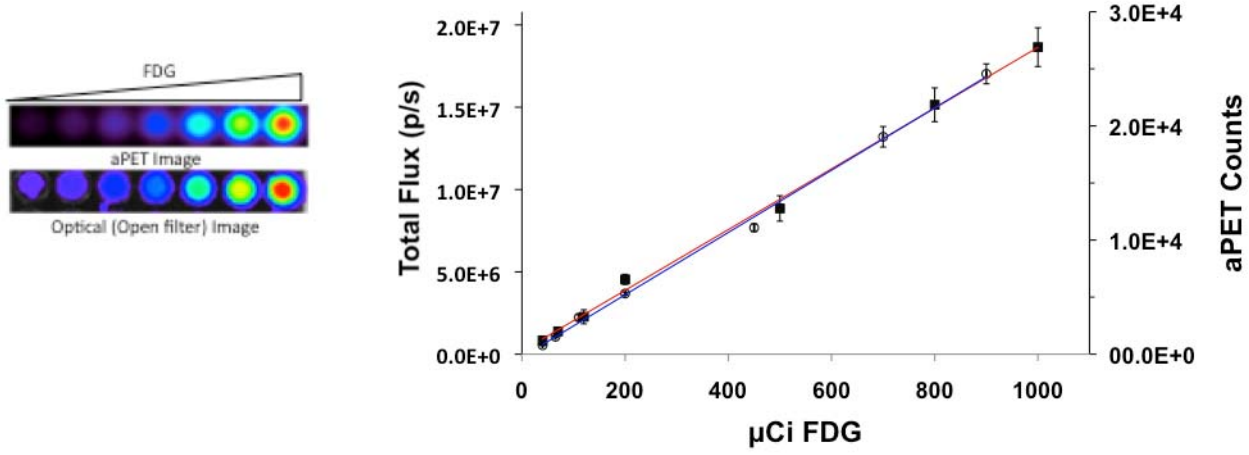

Supplemental Figure 1. Cerenkov emission is linearly dependent on ^{18}F-FDG concentration and correlates strongly with the gamma radiation detected by PET. Left: aPET and Cerenkov optical (open filter) images of a 96-well plate containing dilutions of ^{18}F-FDG ranging from 50-1000 µCi. of ^{18}F-FDG. Right: Graph of Cerenkov photons (closed squares) and aPET counts (open circles) as a function of µCi ^{18}F-FDG concentration (mean of 3 experiments ± standard deviation). The red (R^2 = 0.997) and blue (R^2 = 0.998) lines represent linear fits to the data for optical and PET data respectively.

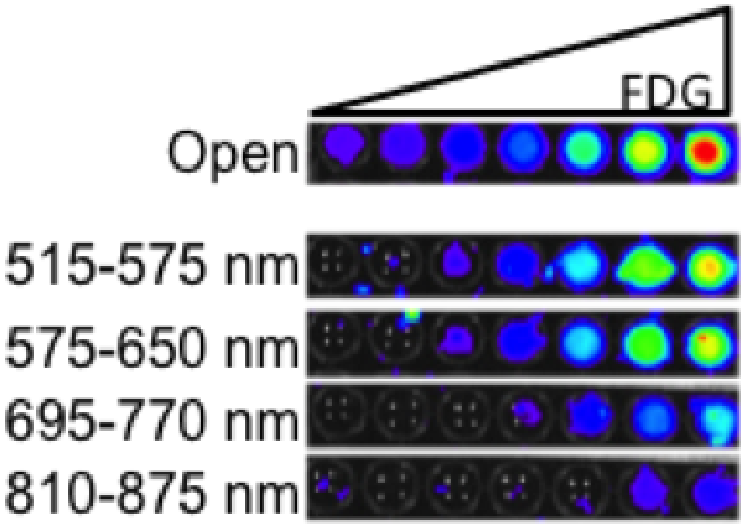

Supplemental Figure 2. Cerenkov emission is blue weighted. Optical images of a serial dilution of FDG (50-1000 μCi) in a 96 well plate taken with open filter and using the 4 emission filters on the IVIS Lumina II. All images (open and filter) are on the same scale. The images show that the majority of the photons are released in the photons were emitted in the 515-575 nm and 575-650 nm range, compared to the NIR range (> 700 nm).

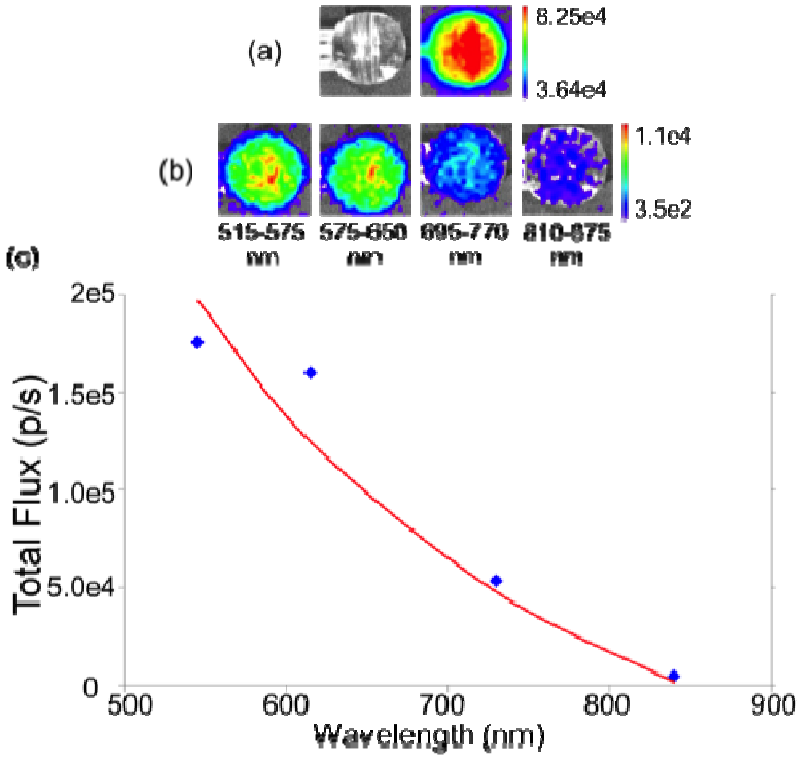

Supplemental Figure 3. Cerenkov emission is multispectral and wavelength dependent (a) White light and open filter images of 27 μCi FDG in a spherical phantom taken on the IVIS Lumina II. (b) Optical images using the selective emission filters. (c) Average radiance for each filter set (blue diamonds). The red line is a theoretical plot of $1/\lambda^2$.

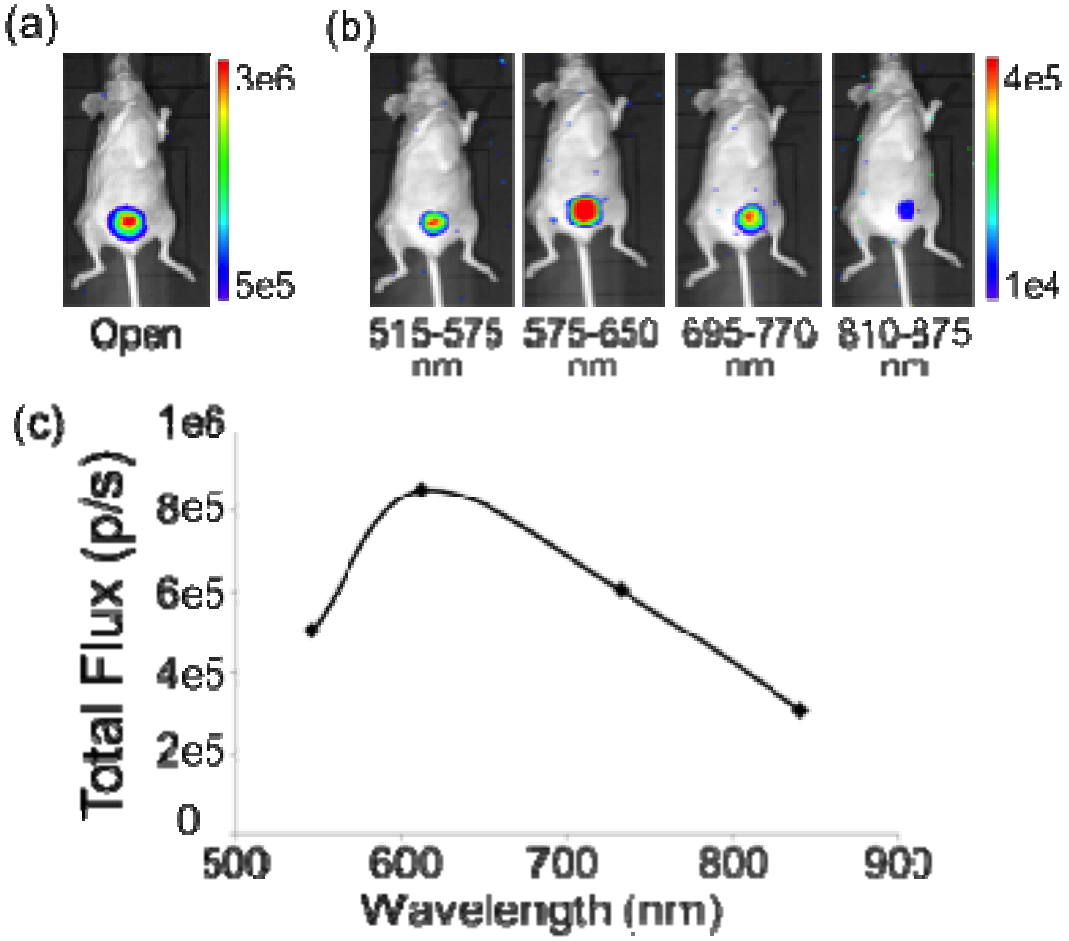

Supplemental Figure 4. Cerenkov emission spectrum of ^{18}F-FDG in vivo. 435 μCi ^{18}F-FDG was administered i.v. into the tail vein of a nude mouse. (a) Optical image using the open filter of the IVIS Lumina II. (b) Optical images using the remaining filter sets. (c) The intensity of the Cerenkov emission in the bladder was quantified and the total flux is shown.

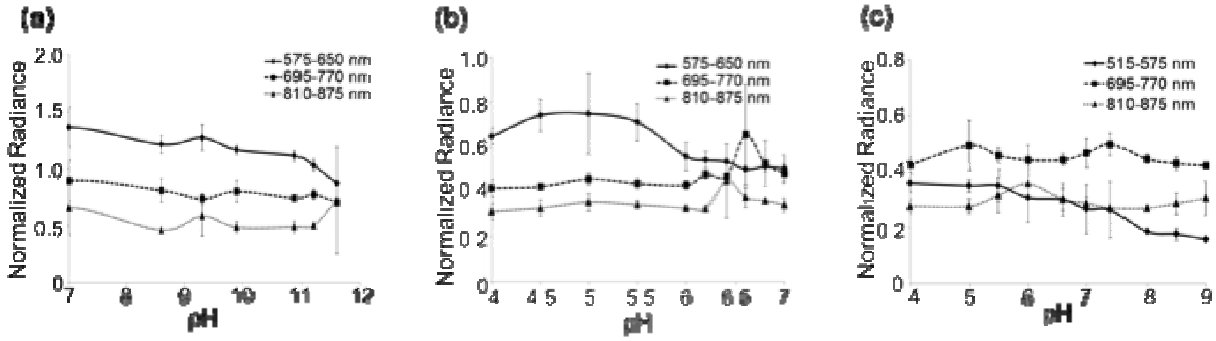

Supplemental Figure 5. Quantification of inter- and intramolecular quenching in well plates. This figure shows quantifications of wells using filters that fall outside the λ_{basic} of the indicators. As a result the changes in Cerenkov emission are relatively unaffected by pH differences. (a) 25 mM PP adjusted to pH 4-11 was mixed with 200 μCi ^{18}F-FDG and imaged using each filter of the IVIS Lumina II. Shown are quantifications of wells using the 575-650 nm, 675-770 nm and 810-875 nm filters. (b) 100 μCi ^{18}F-DFPR was adjusted to pH 4-7 and imaged as in (a). Shown are quantifications of wells using the 575-650 nm, 675-770 nm and 810-875 nm filters. (c) 140 μCi ^{18}F-MFCP was adjusted to pH 4-9 and imaged as in (a). Shown are quantifications of wells using the 515-575 nm, 675-770 nm and 810-875 nm filters. For all experiments, n = 3.